Dynamic assembly and sustained retention of 53BP1 at the sites of DNA damage are controlled by Mdc1/NFBD1

Simon Bekker-Jensen, Claudia Lukas, Fredrik Melander, Jiri Bartek, and Jiri Lukas

Institute of Cancer Biology and Centre for Genotoxic Stress Research, Danish Cancer Society, DK-2100, Copenhagen, Denmark

53BP1 is a key component of the genome surveillance network activated by DNA double strand breaks (DSBs). Despite its known accumulation at the DSB sites, the spatiotemporal aspects of 53BP1 interaction with DSBs and the role of other DSB regulators in this process remain unclear. Here, we used real-time microscopy to study the DSB-induced redistribution of 53BP1 in living cells. We show that within minutes after DNA damage, 53BP1 becomes progressively, yet transiently, immobilized around the DSB-flanking chromatin. Quantitative imaging of single cells revealed that the assembly of 53BP1 at DSBs significantly lagged behind Mdc1/NFBD1, another DSB-interacting checkpoint mediator. Furthermore, short interfering RNA-mediated ablation of Mdc1/NFBD1 drastically impaired 53BP1 redistribution to DSBs and triggered premature dissociation of 53BP1 from these regions. Collectively, these in vivo measurements identify Mdc1/NFBD1 as a key upstream determinant of 53BP1's interaction with DSBs from its dynamic assembly at the DSB sites through sustained retention within the DSB-flanking chromatin up to the recovery from the checkpoint.

Introduction

Protection of genome integrity against mutagenic effects of DNA damage relies on a flawless execution of genome surveillance pathways (so-called "checkpoints") that coordinate cell cycle progression with DNA repair (Zhou and Elledge, 2000; Nyberg et al., 2002). In response to DNA double strand breaks (DSBs), mammalian checkpoints launch a cascade of phosphorylation events initiated by the ataxia-telangiectasia mutated (ATM) protein kinase (Shiloh, 2003). Given its central role in the DSB response, inactivating mutations of *ATM* and/or the genes involved in regulation of ATM activity cause severe genetic disorders manifested by chromosomal instability, radiation sensitivity, and cancer predisposition (Kastan and Bartek, 2004).

A group of proteins named "checkpoint mediators" play a key role in supporting the timely and effective ATM signaling (Lukas et al., 2004b). Among the checkpoint mediators, 53BP1 has recently attracted particular attention (Mochan et al., 2004). Identified originally as a p53-binding protein (Iwabuchi et al., 1994), 53BP1 was later shown to localize to the DSB sites in cells exposed to ionizing radiation (IR) or radiomimetic drugs (Schultz et al., 2000; Anderson et al., 2001). Indeed, several ensuing observations strongly supported a close functional link between 53BP1 and the ATM-regulated events. First, 53BP1 itself becomes phosphorylated by ATM in a DNA damage–dependent manner, suggesting that 53BP1 participates in propagating the ATM signaling to its downstream effectors (Anderson et al., 2001; Ward et al., 2003b). Second, phosphorylation of some ATM targets in 53BP1-deficient mice and human cells is impaired (DiTullio et al., 2002; Wang et al., 2002; Ward et al., 2003a). Third, it has been suggested that 53BP1 may regulate ATM activity by itself (Mochan et al., 2003). Together with the fact that 53BP1 knockout mice suffer from similar (although generally milder) defects as the ATM-deficient mice (Morales et al., 2003; Ward et al., 2003b), the aforementioned findings illustrate that 53BP1 plays an important role in regulating the effectiveness of the ATM-controlled events.

Interestingly, the interaction of 53BP1 with DSBs proceeds in a complex, bimodal fashion. Thus, the assembly at the acute DSB lesions requires direct interaction between the Tudor domain of 53BP1 and dimethylated lysine 79 of histone H3 (H3-dmK79; Huyen et al., 2004). Because this chromatin modification exists in undamaged cells and does not increase in response to DNA damage, it was proposed that chromosomal restructuring adjacent to the DSB lesions locally "unmasks" the

S. Bekker-Jensen and C. Lukas contributed equally to this paper.

Correspondence to J. Lukas: jil@cancer.dk

Abbreviations used in this paper: ATM, ataxia-telangiectasia mutated; DSB, DNA double strand break; H3-dmK79, dimethylated lysine 79 of histone H3; IR, ionizing radiation; MRN, Mre11–Rad50–Nbs1; siRNA, short interfering RNA.

The online version of this article includes supplemental material.

The Journal of Cell Biology, Vol. 170, No. 2, July 18, 2005 201–211
http://www.jcb.org/cgi/doi/10.1083/jcb.200503043

methylated lysine residues, thereby allowing their recognition by 53BP1 (Huyen et al., 2004). After establishing the primary contact with DSBs, the retention of 53BP1 in these regions requires another chromatin modification, the ATM-mediated phosphorylation of histone H2AX on serine 139 (γ-H2AX; Fernandez-Capetillo et al., 2002; Celeste et al., 2003). Unlike H3-dmK79, γ-H2AX is low in undamaged nuclei and becomes rapidly induced by DSB-generating insults in chromatin areas flanking each DSB (Rogakou et al., 1999).

These findings raise important conceptual questions: What is the functional interplay between the H3-dmK79–mediated assembly and γ-H2AX–dependent retention of 53BP1 at the DSB sites? Are these two phases of DSB–53BP1 interaction temporally separated and differently regulated? If so, what is the nature of the molecular switch between them? Furthermore, although H2AX phosphorylation occurs rapidly after DNA damage, how does it becomes relevant for 53BP1 interaction with the DSB regions only later during the DSB response?

To understand the mechanisms (and indeed the purpose) of 53BP1 redistribution after DNA damage, it is important to realize that mammalian cells possess several checkpoint mediators and that all these proteins avidly accumulate in the so-called IR-induced foci. On the one hand, this raises several additional spatiotemporal "problems" such as: How do all these large proteins organize themselves in relatively small areas containing DSBs and limited regions of modified chromatin? Is there a strict "timetable" for an orderly assembly and disassembly of individual checkpoint mediators or do they interact with the DSB microcompartments in a more dynamic and competitive fashion? On the other hand, it is possible that at least some checkpoint mediators may influence each other in terms of their interaction with DSBs and the surrounding chromatin, a notion that might be instrumental to understanding the mechanisms behind early assembly versus late retention of these proteins at the sites of DNA damage. Translated to 53BP1, several papers studied the dependency of 53BP1 accumulation in IR-induced foci as a function of Mdc1/NFBD1 (henceforth Mdc1), another recently characterized checkpoint mediator (Stucki and Jackson, 2004). Although intriguing, these studies reached conflicting results and left a considerable confusion regarding the requirement of Mdc1 for 53BP1 interaction with the DSB sites (Mochan et al., 2004). Thus, whereas two studies reported productive formation of 53BP1-decorated foci (Goldberg et al., 2003; Mochan et al., 2003), another study failed to detect any focal accumulation of 53BP1 in Mdc1-deficient cells after IR (Stewart et al., 2003).

Resolving these issues appears important for several reasons. Most notably, 53BP1 appears to be the closest structural and functional homologue of the "ancestral" checkpoint mediator in unicellular organisms (Rad9 in *Saccharomyces cerevisiae* and Crb2 in *Schizosaccharomyces pombe*, respectively; Mochan et al., 2004). In this sense, deeper insight into its nuclear dynamics may not only clarify the lingering discrepancies about 53BP1 itself but it can also elucidate some of the outlined conceptual questions of how checkpoint mediators interact with DSBs. In the present study, we performed a detailed spatiotemporal analysis of intranuclear redistribution of 53BP1 in its physiological environment: the nucleus of a living mammalian cell. Our results provide new insights into cooperation between Mdc1 and 53BP1 checkpoint mediators in organizing the chromatin microenvironment around the DSBs, help explain the hitherto elusive molecular switch between the assembly and retention of 53BP1 at the DSB sites, and provide evidence for a key role of Mdc1 in mediating sustained interaction of DSB regulators with the DNA damage–modified chromatin.

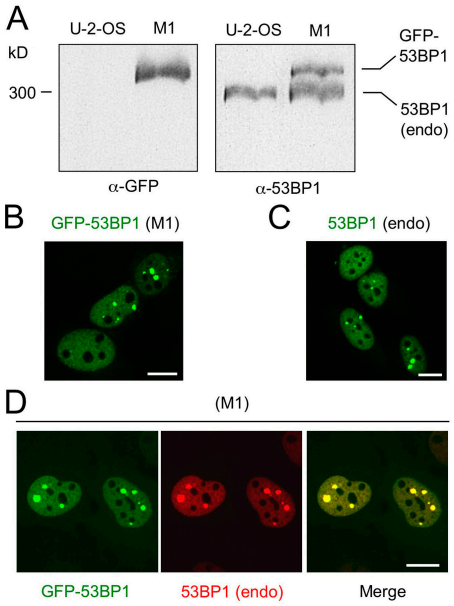

Figure 1. **Characterization of the cellular model to study 53BP1 dynamics in vivo.** (A) Lysates from naive U-2-OS cells and M1 cell line stably expressing murine GFP-53BP1 (25 μg of total protein per lane) were analyzed by immunoblotting with antibodies to GFP (left) and 53BP1 (right). (B) A snapshot of a live, exponentially growing M1 cell line showing nuclear localization of GFP-53BP1 and its accumulation in distinct nuclear speckles in a subset of cells. (C) Naive, asynchronously growing U-2-OS cells were fixed and immunostained with an antibody to endogenous (endo) 53BP1. (D) Exponentially growing M1 cells were immunostained as in C. Note that the accumulation of the endogenous 53BP1 in the nuclear speckles tightly correlates with decoration of these subnuclear compartments with the GFP-tagged protein (in several hundred M1 cells examined by this approach, we never detected a nuclear speckle with endogenous 53BP1 that would not contain also the increased GFP signal). Bars, 10 μm.

Results

A cellular system to study DSB-induced redistribution of 53BP1 in vivo

To investigate spatiotemporal behavior of 53BP1 in live cells, we have generated U-2-OS cell lines stably expressing near-physiological levels of 53BP1 tagged on its NH_2 terminus with the GFP. We have previously shown that U-2-OS cells are proficient in the DSB-induced cell cycle checkpoints and amenable to real-time imaging of DSB-induced protein redistribution (Lukas et al., 2004a). For most experiments in this study, we used the cell line U-2-OS/GFP-53BP1-M1 (henceforth M1) expressing full-length murine 53BP1 (Jullien et al., 2002) tagged with GFP at its NH_2 terminus. This cell line was chosen because the level of GFP-53BP1 matched that of the endogenous protein (Fig. 1 A) and showed little variation in abundance among individual cell nuclei (Fig. 1 B), and the ectopic protein

recapitulated hallmarks of the physiological functions of 53BP1. Thus, the GFP-53BP1 protein migrated with a predicted size on the SDS gels (Fig. 1 A) and showed largely homogeneous, pan-nuclear distribution except for the nucleoli that were void of the protein (Fig. 1 B). In a subset of cells, both GFP-53BP1 in the M1 cell line (Fig. 1 B) and the endogenous 53BP1 in naive U-2-OS (Fig. 1 C) concentrated in one or several bright speckles that likely represent regions with spontaneous DNA damage and/or rearrangements and that were previously described in various human cell types (Mochan et al., 2004). Importantly, the GFP-decorated nuclear speckles always colocalized with those containing the endogenous 53BP1, excluding nonspecific aggregation of the GFP-53BP1 in the M1 cell line (Fig. 1 D). Finally, GFP-53BP1 rapidly relocated to DSBs (generated both by the microlaser and by IR) with very similar kinetics to the endogenous protein (Figs. 2 and 3 and Fig. S1 A, available at http://www.jcb.org/cgi/content/full/jcb.200503043/DC1). The key findings were reproduced in uncloned U-2-OS-GFP-53BP1 cells, and the nuclear mobility of the murine 53BP1 was indistinguishable from its GFP-tagged human counterpart (unpublished data).

Real-time assembly and dynamic exchange of 53BP1 at the DSB sites

Next, we used a real-time assay for monitoring protein assembly at the laser-generated DSB sites, an approach that has provided invaluable insights into protein redistribution and/or modification in response to DSBs (Rogakou et al., 1999; Tashiro et al., 2000; Celeste et al., 2003; Lukas et al., 2003) and that we recently optimized to study these phenomena directly in living mammalian cells (Lukas et al., 2004a). In brief, exponentially growing M1 cells were first presensitized with halogenated thymidine analogues and subsequently microirradiated by a focused UV-A laser beam to generate narrow DSB-containing tracks spanning the entire diameter of cell nuclei. Immediately thereafter, the microirradiated fields were subjected to a time-lapse recording of the GFP-53BP1 protein redistribution (see Materials and methods). Fig. 2 A shows that the assembly of GFP-53BP1 in the DSB-containing nuclear tracks became cytologically discernible after 2 min and reached a steady-state equilibrium between 14–18 min after microirradiation. A very similar kinetic profile was obtained by an immunofluorescence analysis of the endogenous 53BP1 both after laser microirradiation (Fig. 3 C, bottom) and after exposure of a low dose (2 Gy) of IR (Fig. S1 A). These data further support the notion that GFP-53BP1 is biologically active and that the type and extent of the chromosomal lesions generated by the laser are similar to those produced by IR. The detailed mathematical analysis of the GFP-53BP1–associated fluorescence revealed that the assembly of 53BP1 at the DSB sites followed a second order response to a step change, step being defined here as the DSB generation (Fig. 2 B and Table I). The kinetic values (ω) derived from this modelling proved instrumental to directly compare the assembly dynamics between 53BP1 and the related checkpoint mediator Mdc1 (Fig. S2 A, available at http://www.jcb.org/cgi/content/full/jcb.200503043/DC1; and see section The assembly of 53BP1 at the DSB sites lags behind that of Mdc).

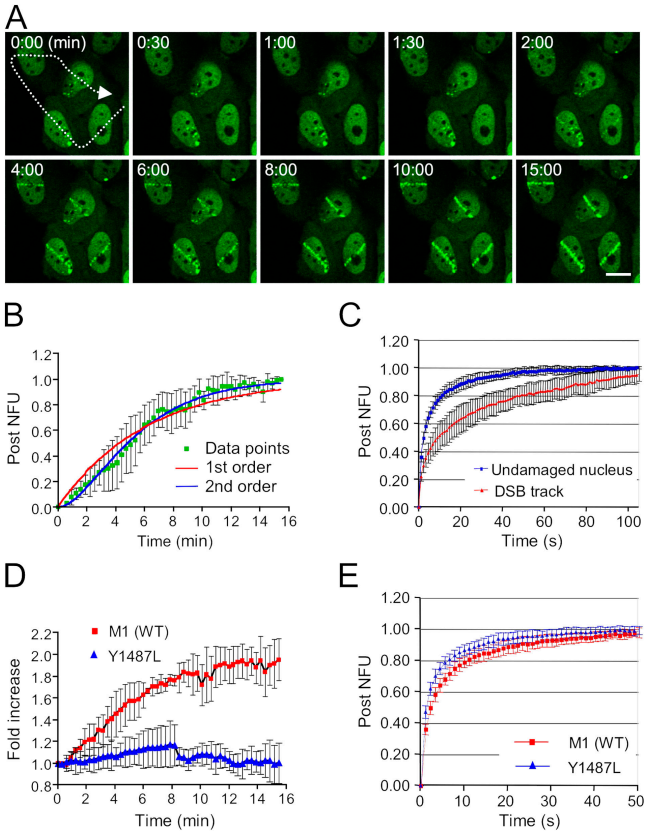

Figure 2. **Dynamic assembly of 53BP1 at the DSB sites.** (A) M1 cells were subjected to laser microirradiation followed by the real-time recording of the GFP-53BP1 assembly kinetics. Dotted arrow in the first image frame indicates the laser paths across the cell nuclei. (B) The M1 cells were assayed as in A, and the fluorescence intensity values reflecting the progressive accumulation of GFP-53BP1 at the DSB sites were recorded, pooled from 10 independent experiments, and fitted to the solutions of linear differential equations of increasing order. NFU, normalized fluorescence units. (C) A summary of the FRAP analysis integrated from 10 independent measurements at the DSB tracks and in undamaged nuclei. Error bars represent twice the SD. (D) Cell lines expressing wild-type (M1) and the Tudor-deficient (Y1487L) forms of GFP-53BP1 were subjected to laser microirradiation as in A. The fold increase in GFP-associated fluorescence along the DSB tracks was calculated and plotted as a function of time. The displayed assembly curves were generated after integrating data from 10 independent experiments for each 53BP1 variant. (E) Undamaged nuclei of M1 and Y1487L cell lines were subjected to FRAP analysis as in C. Note that the recovery profiles are significantly different (compare also the τ values in Table I). Bar, 10 μm.

To gain deeper insight into the 53BP1 interaction with DSBs, we applied FRAP to measure the rate of GFP-53BP1 exchange between the microirradiated nuclear regions and the neighboring nucleoplasm (see Materials and methods). These FRAP measurements revealed that after a single bleach pulse, the GFP-53BP1–associated fluorescence within the DSB tracks recovered with a markedly slower kinetics compared with that in the undamaged nuclei, indicating that a fraction of GFP-53BP1 became transiently immobilized at the DSB sites (Fig. 2 C). Indeed, the mathematical modelling of these FRAP curves supported and further corroborated this conclusion. Thus, the calculated kinetic values (Table I) show that the mobility of GFP-53BP1 could be dissociated into distinct populations with fast- and slow-binding kinetics. Because this pattern

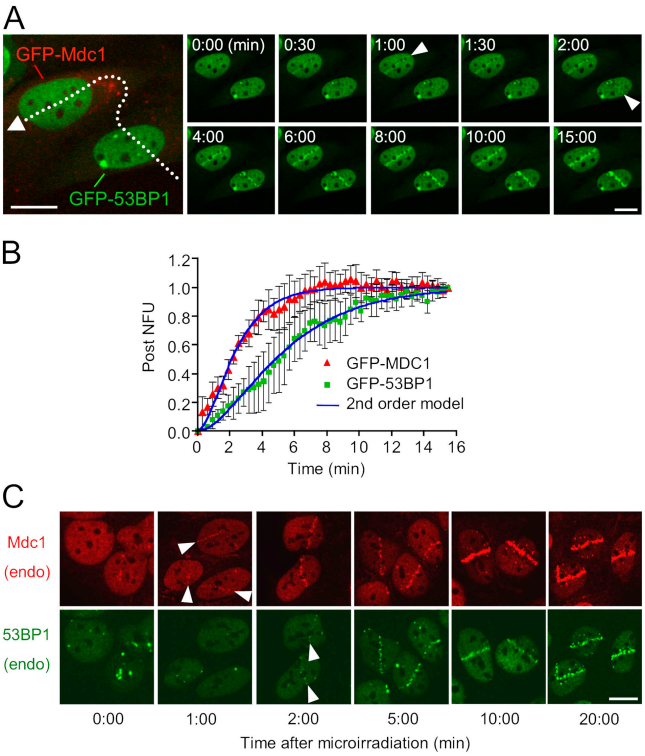

Figure 3. **53BP1 assembly at the DSB sites is delayed compared with that of Mdc1.** (A) U-2-OS cells stably expressing GFP-Mdc1 were labeled with a cytosolic cell tracker (see the extranuclear red fluorescence) and mixed with the GFP-53BP1–expressing cell line. After 24 h, these mixed cell cultures were subjected to laser microirradiation followed by the real-time recording of the GFP-53BP1 and/or GFP-Mdc1 assembly kinetics (dotted arrow indicates the laser paths across the cell nuclei). (B) The kinetic assembly profiles of GFP-Mdc1 and GFP-53BP1 derived from 10 independent experiments (compare also the ω values in Table I). (C) Naive, asynchronously growing U-2-OS cells were plated on grid glass coverslips and microirradiated along a narrow linear region. The exact time of microirradiation was recorded for each individual cell. Immediately after the microirradiation of the last cell, the entire cell population was fixed and coimmunostained with antibodies to Mdc1 (top) and 53BP1 (bottom). The microirradiated regions were retrieved via the coverslip grid and analyzed for the cytologically discernible accumulation of the endogenous proteins in the DSB-containing nuclear tracks. The arrowheads in A and C indicate the time points of the first cytologically detectable accumulation of each protein. Error bars equal twice the SD of the normalized data at the respective time points. Bars, 10 μm.

(including the residence time values for both populations) is reminiscent of several chromatin-associated proteins analyzed by analogous approaches (Phair et al., 2004), these data provide in vivo evidence that even in intact nuclei, 53BP1 dynamically interacts with chromatin. In the microirradiated tracks, this distribution was shifted toward the slower population (39% in undamaged nuclei vs. 58% at the DSB sites; Table I) and the average residence time of this "slow" 53BP1 (the form that presumably binds chromatin with a higher specific affinity) was at least 2.5 times longer at the DSB sites compared with the dispersed protein in the nucleoplasm (Table I). Collectively, these mobility parameters indicate that 53BP1 undergoes a dynamic interaction with chromatin in undamaged cells and that this can be flexibly converted to an increased (yet still transient) immobilization at the DSB sites including the surrounding chromosomal regions.

The Tudor domain determines intranuclear mobility of 53BP1 both before and after DNA damage

Next, we exploited the recent discovery that the Tudor domain of 53BP1 directly interacts with H3-dmK79 (Huyen et al., 2004), thereby determining the productive accumulation of 53BP1 in the IR-induced foci. We have generated another U-2-OS–derived cell line stably expressing GFP-tagged murine 53BP1 with an inactivating mutation (Y1487L) in the core part of the Tudor domain. As predicted, this Tudor-deficient 53BP1 completely failed to assemble along the laser-generated DSB tracks (Fig. 2 D). Surprisingly, FRAP measurements revealed that the Tudor domain disruption accelerated the 53BP1's mobility also in undamaged nuclei manifested by a faster recovery of the GFP-53BP1-Y1487L and a significant decrease of its intranuclear residence time (Fig. 2 E and Table I). Thus, the integrity of the Tudor domain appears to have an impact not only on the ability of 53BP1 to assemble around the DSB lesions but also on its physiological rate of binding to chromatin during unperturbed cell cycle progression (see Discussion).

The assembly of 53BP1 at the DSB sites lags behind that of Mdc1

To gain deeper insight into the dynamics of 53BP1 interaction with DSB-surrounding chromatin, we cross-examined redistribution of 53BP1 and Mdc1 in living cells exposed to the laser-generated DSB tracks. This strategy was inspired by our findings that the assembly of Mdc1 at the DSB sites is required to transiently immobilize the Mre11–Rad50–Nbs1 (MRN) complex (DSB sensor and a key component of early ATM-controlled signaling) in these regions (Lukas et al., 2004a). Given this capacity of Mdc1 to "organize" other proteins within the DSB-flanking chromatin, we tested whether it also contributes to 53BP1 assembly at the DSB sites on a complete checkpoint time scale.

First, we compared the kinetics of 53BP1 and Mdc1 assembly at the freshly generated DSBs. To ensure identical experimental conditions, we cocultivated the GFP-53BP1–expressing M1 cells with U-2-OS cells stably expressing GFP-Mdc1 (Lukas et al., 2004a). To discriminate these two cell lines during imaging (both contain GFP-tagged proteins), we labeled the GFP-Mdc1–expressing cells with a cytosolic cell tracker detectable within the red (λ = 600 nm) emission spectrum (Fig. 3 A; and see Materials and methods). Real-time imaging of these mixed cultures exposed to laser microirradiation revealed that the assembly of GFP-53BP1 in the DSB areas was delayed and proceeded with a significantly slower kinetics compared with that of GFP-Mdc1 (Fig. 3, A and B; and compare ω values in Table I). This temporal difference in Mdc1 and 53BP1 accumulation at the DSB sites was confirmed also for the endogenous proteins analyzed by immunofluorescence in the same cells fixed in short intervals after laser microirradiation (Fig. 3 C). Together, these data suggest that the DSB-associated local chromatin modifications that direct the respective checkpoint mediators to the sites of DNA damage are generated (or become accessible) with different kinetics.

Table I. **Kinetic parameters of 53BP1 and Mdc1**

Real-time assembly (DSBs)		Intranuclear residence time		
ω (min^{-1})		τ (s)		
GFP-Mdc1	0.79 ± 0.02	GFP-53BP1	Fast population	Slow population
		wild type	60% ± 1.0	39% ± 1.0
		(undamaged)	1.6 s ± 0.1	16.0 s ± 0.5
		wild type	40% ± 0.9	58% ± 0.6
		(DSBs)	2.2 s ± 0.1	42.0 s ± 1.7
GFP-53BP1	0.35 ± 0.01	Y1487L	66% ± 0.8	34% ± 0.8
		(undamaged)	1.1 s ± 0.0	11.5 s ± 0.3

See Materials and methods for mathematical modeling.

Mdc1 is required for a productive assembly of 53BP1 at the DSB sites

The aforementioned observation prompted us to investigate whether Mdc1 (the faster DSB interactor) influences the kinetics and/or the magnitude of 53BP1 assembly at the DSB sites. To this end, we quantitatively depleted endogenous Mdc1 in M1 cells by short interfering RNA (siRNA; Fig. 4 A, left) and measured the increase of the GFP-53BP1–associated fluorescence after laser microirradiation. Strikingly, these analyses showed that the saturation amounts of GFP-53BP1 in the microirradiated regions were drastically reduced compared with the Mdc1-proficient cells (Fig. 4 A, right; Fig. 4 B; and Fig. S3, available at http://www.jcb.org/cgi/content/full/jcb.200503043/DC1). Similar impairment in 53BP1 assembly at the DSB sites was observed also in Mdc1-deficient cells exposed to IR (Fig. S1 B). In a reciprocal experiment, an equally quantitative, siRNA-mediated depletion of 53BP1 from the GFP-Mdc1 cells (Fig. 4 C, left) had no significant effect on the kinetics of GFP-Mdc1 assembly around the laser-generated DSBs (Fig. 4 C, right). Together with the aforementioned temporal distinctions between the Mdc1 and 53BP1 assembly kinetics (Fig. 3), and additional FRAP measurements revealing that the Mdc1 depletion reduced the size of the slow binding fraction of GFP-53BP1 in the microirradiated areas (Fig. S2 B), these data suggest that the lack of Mdc1 causes severe limitations for 53BP1 to interact with the DSB sites, including the earliest stages of the DSB response.

To further substantiate this conclusion, we took advantage of our previous results showing that the sustained engagement of Mdc1 with the DSB-flanking chromatin requires γ-H2AX (Lukas et al., 2004a). The clear prediction from these data is that the interference with ATM, the principle DSB-induced kinase involved in H2AX phosphorylation, should not only impair Mdc1 accumulation at the DSB sites but also attenuate the assembly of 53BP1 in these regions. To test this prediction in an isogenic system used for all other kinetic measurements in this study, we knocked down endogenous ATM in the M1 cell line by siRNA (Fig. 5, left). Indeed, ablation of ATM attenuated the assembly of GFP-53BP1 in the laser-generated DSB tracks and the extent of this inhibition was very similar to that achieved by a short pretreatment of cells with caffeine, a drug that under the conditions used (10 mM) inhibits ATM and its close homologue ATR (Fig. 5, right). The fact that the impairment of 53BP1 assembly under these conditions was less dramatic than that obtained by a quantitative Mdc1 ablation is expected given the ability of DNA-PK (another member of the ATM-related kinases) to partially compensate for the lack of ATM in supporting H2AX phosphorylation (Falck et

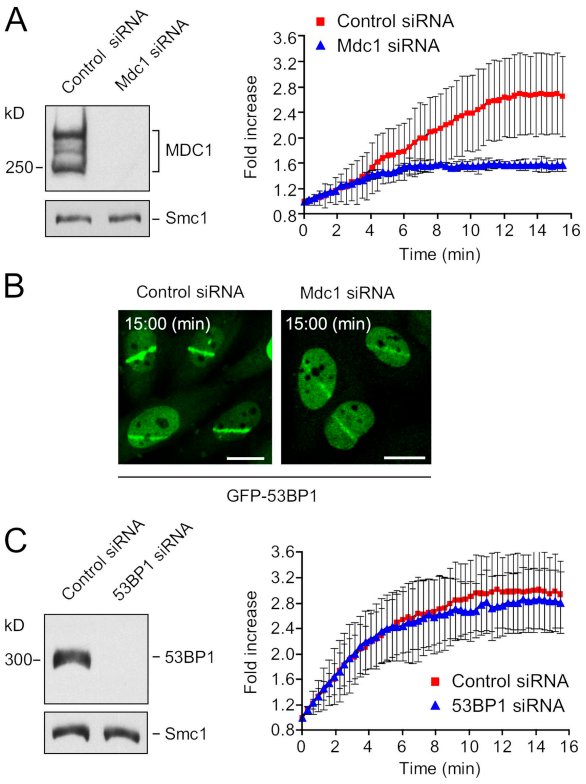

Figure 4. **Impaired assembly of 53BP1 at the DSB sites in the absence of Mdc1.** (A) Lysates from M1 cells transfected with control- or Mdc1-directed siRNA duplexes for 72 h were analyzed by immunoblotting with the indicated antibodies (left). In parallel, the siRNA-treated cells were microirradiated and subject to the real-time assembly measurement of GFP-53BP1 as in Fig. 2 A (right). The fold increase in GFP-associated fluorescence along the DSB tracks was calculated and displayed as in Fig. 3 B. (B) A snapshot of live M1 cells treated with the indicated siRNA duplexes as in A and recorded 15 min after laser microirradiation. Note the reduced intensity of the GFP-53BP1–associated fluorescence at the DSB areas in Mdc1-depleted cells. (C) Lysates from a GFP-Mdc1–expressing cell line transfected with control- or 53BP1-directed siRNA duplexes were analyzed by immunoblotting with the indicated antibodies (left). 72 h after siRNA transfections, the cells were microirradiated and subjected to the real-time assembly measurement of GFP-Mdc1 (right). Smc1 immunoblots in A and C serve as loading controls. All kinetic experiments in this figure were derived from three independent experiments with 10 cells evaluated for each condition. Error bars equal twice the SD of the normalized data at the respective time points. Bars, 10 μm.

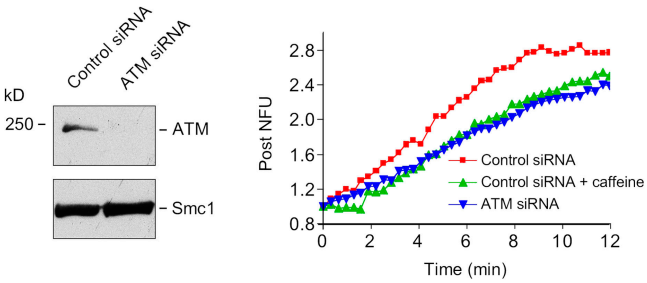

Figure 5. **Inhibition of the ATM kinase recapitulates the impact of Mdc1 down-regulation on the 53BP1 assembly at the DSB sites.** M1 cells were treated with control or ATM-targeting siRNA duplexes for 72 h and analyzed by immunoblotting for the efficiency of ATM down-regulation (left; Smc1 immunoblot serves as a loading control). In parallel, the siRNA-treated cells were subject to local laser microirradiation followed by the real-time recording of the GFP-53BP1 assembly kinetics (right). Where indicated, caffeine (10 mM) was added to the culture media immediately before microirradiation.

al., 2005). Thus, these data strengthen the notion that the efficient 53BP1 assembly requires the preceding formation of the γ-H2AX–Mdc1 complex at the DSB sites and indicate that one of the important functions of ATM is to stabilize otherwise transient (or inefficient) protein interactions with the sites of DNA damage.

Mdc1 is required for a sustained retention of 53BP1 at the DSB sites

Next, we investigated the dynamics of 53BP1 interaction with DSBs (and the role of Mdc1 in this process) during the advanced stages of the DSB response, spanning the checkpoint maintenance and recovery. We extended the real-time recording of microirradiated M1 cells for several hours and confirmed that under our experimental conditions, the extent of DNA damage did not exhaust the cellular capacity to repair the DSB lesions. Indeed, we could generate conditions compatible with uninterrupted, single cell–based imaging of a complete disassembly of GFP-53BP1 from the microirradiated tracks followed by apparently normal mitosis (Fig. 6 A). The division of the microirradiated cells was delayed compared with otherwise unstressed cells assayed under the same conditions, but the majority of the laser-treated cells remained viable, consistent with inducing a bona-fide cell cycle checkpoint by the local DSB tracks (Table II). We then used this approach to measure dissociation of GFP-53BP1 from the DSB regions by determining the time when the GFP-53BP1–specific fluorescence in the microirradiated tracks reequilibrated with that in the undamaged parts of the same nucleus. These time-lapse analyses revealed that Mdc1 was critically required for a sustained interaction of 53BP1 with these regions (Fig. 6 B). Thus, the bulk of the Mdc1-proficient cells lost GFP-53BP1 from the DSB tracks between 7 and 12 h after microirradiation. In contrast, depletion of the endogenous Mdc1 not only impaired the magnitude of GFP-53BP1 assembly at the DSB sites (Fig. 4, A and B; and Figs. S1 B and S3) but also reduced the overall period of the cytologically discernible GFP-53BP1 accumulation in these regions to <6 h. In fact, the majority of these Mdc1-deprived cells completely lost GFP-53BP1 from the DSB sites already 2 h

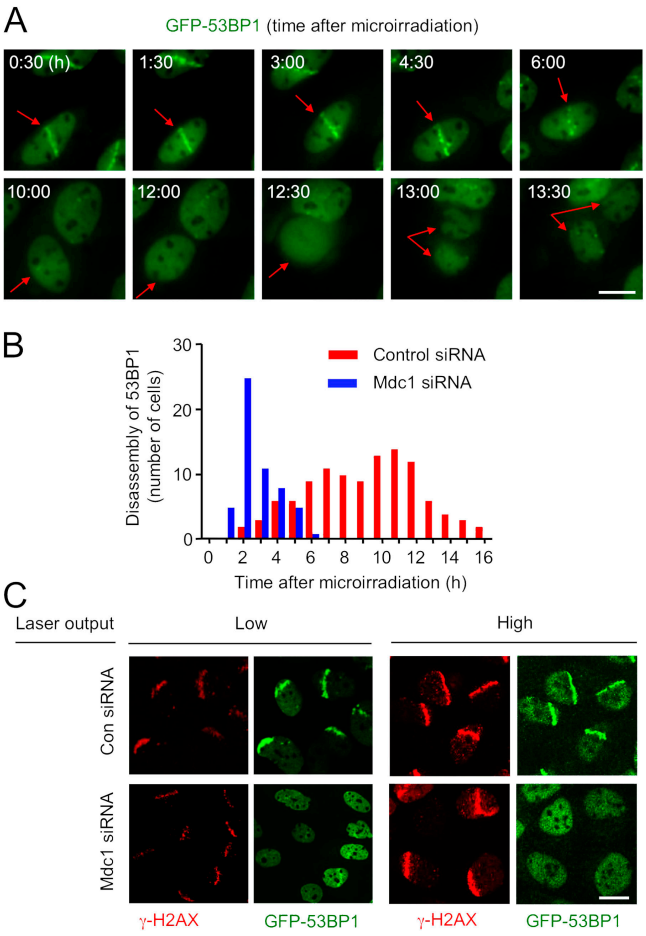

Figure 6. **53BP1 undergoes premature dissociation from the DSB sites in the absence of MDC1.** (A) M1 cells were microirradiated as described in Fig. 2 A and subject to an extended time-lapse recording. Red arrows trace a cell where GFP-53BP1 progressively dissociated from the DSB tracks and which then underwent a complete mitosis. (B) M1 cells were treated with control- and Mdc1-directed siRNA for 72 h, microirradiated, and subject to the extended time-lapse analyses as in A. The disassembly rate of GFP-53BP1 from the DSB tracks was assessed by recording the time when the GFP-associated fluorescence in the DSB areas equilibrated with that in the undamaged parts of the same nucleus. (C) M1cells were treated with the indicated siRNAs and microirradiated with the low and high laser energy output to generate an increasing amount of DNA damage (see Materials and methods). 4 h after microirradiation, the cells were fixed and immunostained with an antibody to γ-H2AX. Note that the Mdc1 depletion drastically impaired GFP-53BP1 interaction with the DSB sites at the time when focal accumulation of γ-H2AX remained clearly discernible in these regions. Bars, 10 μm.

after microirradiation (Fig. 6 B). This unscheduled dissociation of 53BP1 in microirradiated Mdc1-deprived cells was accompanied by a complete lack of normal cell division and by markedly decreased cell viability (Table II). Also in this case, we validated the data obtained by laser microirradiation with an independent source of DSB. Indeed, very similar results (marked impairment of GFP-53BP1 interaction with DSBs in later stages of the checkpoint response) were obtained in cells exposed to low doses (2 Gy) of IR (Fig. S1 B). Importantly, the premature dissociation of 53BP1 in Mdc1-deficient cells was not a simple consequence of its inefficient assembly. When we increased the laser output to generate more DSBs and thereby

Table II. **Cellular responses to the indicated siRNAs and/or laser microirradiation**

	Normal mitosis	No cell division viable cells	Cell death
No microirradiation; No siRNA (n = 129)	90%	4%	6%
Microirradiated; No siRNA (n = 202)	21%	62%	17%
Microirradiated; Control siRNA (n = 140)	10%	67%	23%
Microirradiated; Mdc1 siRNA (n = 167)	0%	40%	60%

Assayed during 40 h of continuous time-lapse imaging.

elevate the relative abundance of GFP-53BP1 in the microirradiated tracks to the level achieved by a lower laser dose in control cells, GFP-53BP1 was still lost several hours earlier in cells without Mdc1 (Fig. S4, available at http://www.jcb.org/cgi/content/full/jcb.200503043/DC1).

It has been reported by others in IR-treated cells (Stewart et al., 2003) and noticed by ourselves after laser microirradiation (this study) that the abundance of γ-H2AX at the DSB sites was somewhat reduced in the Mdc1-depleted cells (this phenomenon was more pronounced after low irradiation doses and at later time points; Fig. 6 C). In addition, H2AX is required for the sustained interaction of 53BP1 at DSBs (Celeste et al., 2003). This raises the important conceptual question of whether Mdc1 regulates the assembly of 53BP1 directly (for instance by actively promoting chromatin rearrangements; see Discussion) or indirectly through its impact on the extent of H2AX phosphorylation. To discriminate between these possibilities, we analyzed γ-H2AX and GFP-53BP1 colocalization at multiple time points after Mdc1 depletion and local microirradiation of M1 cells with the increasing laser energy output (to generate moderate and high DNA damage within the laser-exposed nuclear regions). Importantly, these immunofluorescence analyses identified a clear time window (between 3 and 4 h after microirradiation) when γ-H2AX was still clearly present in the DSB tracks (especially apparent after high irradiation dose), whereas GFP-53BP1 became completely dispersed throughout the nucleoplasm (Fig. 6 C). Together, these data strongly suggest that the productive assembly and/or maintenance of 53BP1 in the DSB-flanking chromatin cannot be achieved by γ-H2AX alone and support the central role of Mdc1 in bridging the γ-H2AX–marked chromatin with the sustained engagement of 53BP1.

Discussion

Our data provide in vivo evidence that without Mdc1 the interaction of 53BP1 with the DSB-surrounding chromatin is rather inefficient and that the time period during which 53BP1 gains access to the DSB sites is substantially shortened. Specifically, Mdc1-deficient cells never accumulate 53BP1 in the DSB areas

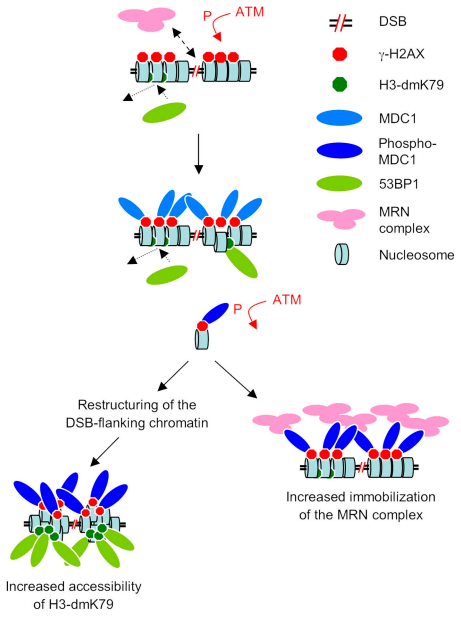

Figure 7. **Model of the spatiotemporal organization of the chromosomal microcompartments surrounding the DSB sites.** DSB detection by the MRN complex is followed by the recruitment of active ATM and phosphorylation of H2AX in the DSB-flanking chromatin. At this stage, H3-dmK79 remains poorly accessible and allows only a very transient 53BP1–chromatin interaction (top). Generation of γ-H2AX triggers assembly of Mdc1. The physical changes in the DSB-surrounding chromatin also initiate accumulation of 53BP1 by an increased exposure of a limited number of H3-dmK79 residues. However, this interaction is relatively inefficient and manifests by a temporal delay of 53BP1 assembly compared with that of Mdc1 (middle). Continuing accumulation of γ-H2AX–Mdc1 complexes in the DSB regions followed by ATM-dependent phosphorylation of Mdc1 triggers the full-scale assembly of 53BP1. This may be achieved either by promoting further structural rearrangements of the DSB-surrounding chromatin compatible with an increased exposure of interaction-competent H3-dmK79 residues (bottom, left) or by stabilization of the 53BP1-H3-dmK79 binding. In parallel, accumulation of ATM-phosphorylated Mdc1 in the vicinity of the DNA lesions stabilizes the interaction of the MRN complex with these regions via direct protein–protein interaction (bottom, right; see Discussion).

to physiological levels and they tend to lose 53BP1 from these regions several hours before restoration of the DNA and/or chromatin integrity. Together with our previous kinetic measurements of Mdc1 (Lukas et al., 2004a), these results help reconcile the current discrepancies in terms of Mdc1-53BP1 interplay in DSB interaction (Introduction) and begin to shed light on the quantitative and temporal aspects of the DSB-surrounding chromatin organization in living mammalian cells. The salient points of the current model (Fig. 7) are as follows.

In the context of intact nucleosomes, the H3-dmK79 residues are poorly accessible and support only very transient interaction of 53BP1 with chromatin. After generation of DSBs and their recognition by the MRN complex, recruitment of active ATM generates areas of γ-H2AX in the vicinity of the DNA lesions. This provides a high-affinity template for a rapid and quantitative assembly of Mdc1 in the DSB-flanking chromatin. Interruption of DNA integrity is likely accompanied also by local physical alterations of the surrounding chromatin (such as changes in tension within a given chromosomal domain) that may increase exposure of a limited amount H3-dmK79 residues and thereby promote immobilization of a small amount of

53BP1. This explains why several previous studies concluded that 53BP1 could be seen in IR-induced foci in the absence of Mdc1 (Goldberg et al., 2003; Mochan et al., 2003). However, we would like to emphasize that this degree of 53BP1 accumulation at DSBs is grossly subphysiological and transient; the latter finding providing a likely explanation for why another study failed to detect focal accumulation of 53BP1 several hours after DNA damage in Mdc1-depleted cells (Stewart et al., 2003). Our quantitative real-time measurements strongly suggest that only after assembly of a threshold amount of Mdc1 around the DSB sites, and presumably also by its phosphorylation by ATM (see the following paragraphs and Fig. 7), the DSB-surrounding chromatin undergoes large-scale structural changes necessary and sufficient for the unrestrained accessibility of H3-dmK79 followed by a full-scale assembly of 53BP1 (Fig. 7). Whether the increased exposure of H3-dmK79 reflects a local chromatin relaxation (thereby "unmasking" the otherwise hidden parts of the nucleosomes) or a higher degree of chromatin compaction as recently proposed (Fernandez-Capetillo et al., 2004; the latter may concentrate the otherwise "scattered" H3-dmK79 residues to the vicinity of the primary DSB lesions) remains to be elucidated. In either case, the key addition of the present study to this model is the evidence that accumulation of a critical amount of Mdc1 at the DSB sites appears to serve as a molecular switch converting the inefficient assembly of 53BP1 at the DSB sites to its robust and sustained engagement with the DSB-surrounding chromosomal regions.

In addition to integrating 53BP1 to the spatiotemporal "map" of the DSB response, interesting conclusions could be derived from the analysis of its mobility in undamaged nuclei. The distribution of the nuclear pool of 53BP1 into fast and slow moving fractions (Table I) indicate that even in the absence of DNA damage 53BP1 associates with chromatin (Phair et al., 2004). This basal 53BP1–chromatin interaction is transient (thereby allowing relatively rapid movement and availability of a sizable pool of 53BP1 throughout the nucleus), it is partly dependent on the integrity of the methyl-binding Tudor domain (suggesting that H3-dmK79 could be transiently exposed during unperturbed cell cycle, likely as a result of the dynamic conformational changes of nucleosomes; Li et al., 2005), and could be instantly converted to a more sustained immobilization of 53BP1 at the acutely emerging sites of DNA breaks. Such protein redistribution after DNA damage is not unprecedented. Rapid movement of repair factors and their transient immobilization after stochastic collisions with DNA lesions was originally described for proteins involved in the nucleotide excision repair (Houtsmuller et al., 1999) and later confirmed as a prevailing way of protein communication with other types of DNA lesions including DSBs (Essers et al., 2002; Lukas et al., 2003, 2004a).

How does Mdc1 influence 53BP1 redistribution? One parameter that can explain the gain of Mdc1's ability to organize 53BP1 and other proteins specifically in the context of DNA damage is its own, ATM-mediated phosphorylation (Stucki and Jackson, 2004). This idea was originally inspired by our finding that the switch between transient interaction and sustained accumulation of MRN at the DSB sites requires both Mdc1 and the intact FHA domain of Nbs1 (Lukas et al., 2004a). As the FHA domains bind DNA damage-induced phosphothreonines (Durocher et al., 2000), it is likely that both physical presence and phosphorylation of Mdc1 determine the increased immobilization of Nbs1 in the DSB regions (Fig. 7). Although the 53BP1 contains a tandem BRCT domain, which is an equally avid phosphothreonine interactor (Manke et al., 2003; Yu et al., 2003), its accumulation at the DSB sites seems to differ from the Mdc1-Nbs1 interplay, because deletion and/or mutation of the BRCT domains neither changed the assembly nor modified the residence time of 53BP1 at the DSB sites (unpublished data). Instead, we propose that after its assembly around DSBs and phosphorylation by ATM, Mdc1 gains the ability to facilitate the recruitment of chromatin-remodelling enzymes (Fig. 7), such as those that had been reported to interact with phosphorylated histone H2A in yeast (Downs et al., 2004; Morrison et al., 2004; van Attikum et al., 2004). The ensuing nucleosomal rearrangements may then promote and/or stabilize exposure of H3-dmK79. An alternative (but not mutually exclusive) scenario is that the presence of phosphorylated Mdc1 at the DSB-flanking chromatin directly stabilizes binding between 53BP1 and interaction-competent H3-dmK79 residues. Thus, together with the recent biochemical evidence for its ability to integrate multiple DSB regulators at the sites of DNA damage (Goldberg et al., 2003; Lou et al., 2003b; Peng and Chen, 2003; Stewart et al., 2003; Xu and Stern, 2003), Mdc1 appears to perform a key role in organizing the DSB-surrounding chromosomal microenvironment, a function that may have important biological ramifications. In particular, the inability to concentrate proteins such as MRN and 53BP1 at the DSB sites in Mdc1-deficient cells could impair timely and productive DSB repair and thereby explain the decreased survival of such cells reported previously in clonogenic assays (Lou et al., 2003a; Stewart et al., 2003) and confirmed in this study by the real-time imaging of individual cells (Table II).

Finally, the quantitative and temporal aspects of our measurements, combined with a direct comparison of intranuclear protein redistribution under identical experimental conditions, challenge another intensively debated issue, namely the nature of the mechanisms that sense DSB lesions and initiate the genome surveillance program. In particular, it has been proposed that Mdc1 and 53BP1 constitute two branches of cellular mechanism to activate ATM-dependent signaling in cells exposed to DSBs (Mochan et al., 2003). However, our new data showing that the assembly of 53BP1 at the freshly generated DNA lesions lags behind Mdc1 and that the proficient 53BP1-DSB assembly is indeed dependent on Mdc1 are not consistent with 53BP1 being the prime sensor of DSBs. Moreover, our previous results strongly suggest that Mdc1 is not involved in the initial DSB detection either. The key arguments here are that Mdc1 is not a constitutive structural component of the MRN complex (the likely DSB sensor; see the following paragraph) and that the interaction of Mdc1 with the DSB-flanking chromatin is critically dependent on the H2AX phosphorylation (i.e., downstream of at least the first "wave" of ATM activity; Lukas et al., 2004a). Instead, our data indicate that both Mdc1 and 53BP1 function as genuine "mediator" and/or

"adaptor" proteins and that their main role is to enhance and locally concentrate the efficiency of multiple interactions between activated ATM and its substrates, thereby facilitating the pace and velocity of the ATM-controlled signaling.

What, then, is the true DSB sensor? Kinetic measurements in yeast (Lisby et al., 2004) and our own results in mammalian cells (Lukas et al., 2004a) revealed that so far the only nuclear factor whose productive interaction with DSBs does not seem to require other proteins and/or protein modifications and whose arrival at the freshly generated DSBs precedes that of all DSB regulators analyzed so far is the MRN (MRX in *S. cerevisiae*) nuclease complex. Unlike 53BP1, the MRN complex has a distinctly dual mode of interaction with the DSB sites, including direct and transient binding to DNA (D'Amours and Jackson, 2002) and the more sustained, chromatin-dependent accumulation in the DSB-flanking chromatin (Lukas et al., 2004a). Although the first mode (Mdc1 independent) is compatible with the proposed role of MRN as a DSB sensor, the second one (Mdc1 dependent) likely serves other purposes such as preventing dispersal of the ATM-activated MRN to the undamaged nuclear compartments (Lukas et al., 2004a). In contrast, the recent biochemical analyses (Huyen et al., 2004) revealed no evidence for the direct interaction of 53BP1 with DNA, a notion fully consistent with our present single cell–based approach. Thus, unlike the MRN complex (that can interact with DSBs in both DNA-dependent and chromatin-dependent modes), the productive assembly of 53BP1 at DSBs relies on a single interaction mode that is largely (if not exclusively) dependent on temporally preceding chromatin modifications, specifically on the formation of the γ-H2AX–Mdc1 complex. Together, this strongly suggests that although 53BP1 may reinforce DSB signaling, it is not the primary DSB sensor.

Materials and methods

Plasmids

The expression plasmid for mouse GFP-53BP1 was a gift from Y. Adachi (The University of Edinburgh, Edinburgh, UK; Jullien et al., 2002). A point mutation resulting in a substitution of tyrosine 1487 of the Tudor domain to leucine (Y1487L) was generated by PCR using the Quick Change Kit (Stratagene).

Cell culture and RNA interference

For generation of stable cell lines, the human U-2-OS osteosarcoma cells (American Type Culture Collection) were cotransfected with the expression plasmids containing various forms of GFP-53BP1 and the pBabe-puro containing the puromycin resistance cassette. Upon selection with 1 μg/ml puromycin (Sigma-Aldrich) for 10 d, resistant clones were tested for the expression and functionality of the GFP-tagged proteins. The U-2-OS–derived cell line stably expressing GFP-Mdc1 was described previously (Lukas et al., 2004a). For live-cell experiments, the cells were plated on the Lab-Tek chambered coverglass (Nunc) or on Cellocate grid coverslips (Eppendorf). The culture medium was supplied with 10 μM BrdU (Sigma-Aldrich) for 24 h to sensitize the cells for DSB generation by UV-A laser (Lukas et al., 2003, 2004a). For every live-cell manipulation and/or recording, the cells were supplied with a phenol red-free, CO_2-independent medium (Invitrogen). For distinction of GFP-53BP1– and GFP-Mdc1–expressing cells during simultaneous imaging of mixed cell cultures, the GFP-Mdc1 cell line was labeled with the red-emitting CMTPX Cell Tracker (Molecular Probes) according to the manufacturer's instructions. IR was delivered by X-ray generator (Pantak HF160, 150kV, 15mA, dose rate 2.18 Gy/min) as described previously (Syljuasen et al., 2004). The Mdc1-targeting siRNA duplexes were described previously (Lukas et al., 2004a). The 53BP1-targeting siRNAs were designed and used as described in DiTullio et al. (2002). The ATM-targeting siRNA was a Smartpool (Dharmacon). Control siRNA (5′-gggaggacaagacguucua-3′) was against HSP70B (Leung et al., 1990), a variant of the human heat shock protein that is not expressed in U-2-OS cells. All siRNAs were synthesized by Dharmacon research.

Antibodies and immunochemical techniques

Mouse mAbs against 53BP1 and ATM (MAT3) ware gifts from T. Halazonetis (Wistar Institute, Philadelphia, PA; Schultz et al., 2000) and Y. Shiloh (Tel Aviv University, Tel Aviv, Israel), respectively. Additional antibodies used in this study included: rabbit anti-Smc1 (Abcam), rabbit anti-GFP (Santa Cruz Biotechnology, Inc.), rabbit anti-53BP1 (Oncogene Research Products), rabbit 53BP1 (Santa Cruz Biotechnology, Inc.), rabbit and mouse anti–γ-H2AX (Upstate Biotechnology). Rabbit antibody to Mdc1 was provided by S. Jackson and M. Stucki (The Wellcome Trust/Cancer Research Institute, Cambridge, UK; Goldberg et al., 2003). Highly cross-adsorbed secondary antibodies for immunofluorescence coupled to Alexa 488 or Alexa 568 were purchased from Molecular Probes. Conditions for immunostaining, SDS-PAGE electrophoresis, and immunoblotting were described previously (Falck et al., 2002; Lukas et al., 2003, 2004a).

Microscopy

Confocal microscopy of fixed cells was performed on LSM 510 (Carl Zeiss MicroImaging, Inc.) mounted on a microscope (model Zeiss-Axiovert 100M; Carl Zeiss MicroImaging, Inc.), equipped with Plan-Neofluar 40×/1.3 oil immersion objective, and with appropriate configurations for multiple color acquisition. For live cell confocal microscopy, a custom-designed imaging workstation combining the LSM 510 Meta (Carl Zeiss MicroImaging, Inc.) and the P.A.L.M. microdissector (PALM Robotics) was used. A 40×/1.2 C-Apochromat water immersion objective was used both for microirradiation and image acquisition. Generation of local DSB regions by laser microirradiation and the FRAP assays were described previously (Lukas et al., 2003, 2004a). Given these objective parameters the energy output of the microdissection laser that is compatible with generating local DSB tracks ranges between 51, 55, and 59%, yielding low, intermediate, or high concentration of local DSBs (Lukas et al., 2003). Unless stated otherwise, the 55% laser energy output was used. Time-lapse experiments were performed on a widefield fluorescence microscope (Axiovert 200; Carl Zeiss MicroImaging, Inc.) equipped with Plan Neofluar 25×/0.8 oil immersion objective, a charge-coupled device camera (Coolsnap HQ; Roper Scientific), and Metamorph software (Universal Imaging Corp.). A typical time-lapse acquisition protocol consisted of a 5-min interval autofocus on a differential interference contrast transmission light image (10-ms exposure time) followed by one snapshot of a GFP image with an exposure time of 100 ms. All microscopes used for live cell imaging were equipped with a 37°C tempered XL incubator and the culture medium was overlaid with mineral oil to prevent evaporation. For quantitative and comparative imaging, identical image acquisition parameters were used. Software packages used to capture the images, analyze the data, and generate the graphs included LSM (Carl Zeiss MicroImaging, Inc.), Metamorph (Universal Imaging Corp.), Excel (Microsoft), and Prism 4 (Graphpad Software).

Real-time assembly assays

Operation of the combined confocal and microdissection microscope was performed essentially as described previously (Lukas et al., 2003, 2004a), with the addition that time-lapse series for dynamic measurements of DSB-induced protein redistribution were acquired as sets of 50 pictures averaged four times (acquisition time = 4 s) with intervals of 15 s between individual frames. Fluorescence redistribution data from regions encompassing the irradiated tracks of at least 10 cells per experiment were extracted from these time-lapses. The fluorescence values of individual frames were annotated so that I_t denotes the intensity of the measured region at time point t, whereas I_o and I_∞ denote the values measured in the first and last frame, respectively. Additionally, three values for each measured cell were recorded: (1) background fluorescence outside the nucleus (I_{bg}), (2) basal intensity within the nucleus in the first frame (I_{pre}), and (3) the peak intensity within the DSB track in the last frame (I_{end}). These data were combined in two different ways to normalize the fluorescence output from individual cells. In the first way, post-normalization of fluorescent units (Post NFU) translates the data into a kinetic profile of numbers between 0 and 1. These numbers were used for mathematical modelling in the following equation: Post NFU = $(I_t - I_o)/(I_\infty - I_o)$. The second way was fold increase normalization, which is an absolute measure for the increase in fluorescence within the DSB-containing nuclear regions over time. In this case, the mathematical evaluation of the data was done as follows: Fold increase = $1 + [\text{Post NFU} \times (I_{end} - I_{pre})/(I_{pre} - I_{bg})]$.

For kinetic modelling, post value normalized data were fitted to solutions of linear differential equations of increasing order. Thus, the two following one-parameter first and second order, respectively, kinetic models for the redistribution profiles were considered:

$$y(t) = 1 - \exp(-t/\tau)$$

$$y(t) = 1 - \exp(-\omega \times t) - \omega \times t \times \exp(-\omega \times t)$$

Application of the second order model gave the best fit using the Prism 4 software. Therefore, the ω parameter was used to compare the protein's assembly kinetics for various conditions specified in the figure legends. The same mathematical procedure was applied to model real-time assembly of Mdc1 (Fig. S2 A). In this case, both the first and second order model fitted well the experimental data (Lukas et al., 2004a), and the second order model was used here to directly compare the kinetic assembly of Mdc1 with that of 53BP1 (the latter could be satisfactorily described only by the second order model [Fig. 2 B]).

Photobleaching protocols

The nuclei of M1 cells were microirradiated, and the GFP-53BP1 protein was allowed to reach its maximal steady-state concentration in the DSB-containing nuclear tracks (typically 20 min after laser exposure). Subsequently, a narrow, 2-μm-wide rectangular region was placed over the entire DSB track and/or the undamaged nucleoplasm as indicated in the figure legends. After acquisition of five prebleach images, this region was subjected to a single bleach pulse of five iterations at a laser transmission of 100%. Subsequently, 95 images were acquired in 1-s intervals with 0.5% laser transmission. Averaged fluorescence intensities of the whole or parts of these regions were extracted and normalized either to the post-bleach value (see Post NFU equation in previous section) or to the pre-bleach value as follows: Pre NFU = $(I_t - I_o)/(I_{pre} - I_o)$. In the latter case, I_o stands for the intensity in the first frame after the bleach pulse, I_∞ for the average of the five last measurements, and I_{pre} for the average of the five prebleach measurements. Post-normalized fluorescence (see Post NFU equation in previous section) values from the strip FRAP experiments were used for kinetic modelling. Assuming two populations of binding reactions between mobile 53BP1 and immobile chromatin, the relative abundance (Y) of the 53BP1 populations engaging in the different binding reactions and the time spent within the bleach region (τ) of protein molecules from each population were modeled for different proteins and conditions according to the following equation (Schmiedeberg et al., 2004):

$$y(t) = Y_1(1 - \exp(-t/\tau_1)) + Y_2(1 - \exp(-t/\tau_2))$$

Online supplemental material

Fig. S1 shows that the timing of GFP-53BP1 assembly in the IR-induced foci recapitulates that of the endogenous protein and that Mdc1 ablation by siRNA attenuates formation of the GFP-53BP1 foci. Fig. S2 shows the kinetic modeling of GFP-Mdc1 assembly at the microlaser-generated DSB sites and the impaired binding of GFP-53BP1 to the DSB-flanking chromatin in Mdc1-depleted cells assayed by FRAP. Fig. S3 shows the inefficient assembly of GFP-53BP1 in a microirradiated Mdc1-deficient cell when compared with an Mdc1-proficient cell recorded in the same microscopic field. Fig. S4 shows that the lack of Mdc1 triggers premature dissociation of GFP-53BP1 from the sites of extensive DNA damage generated by high-energy laser irradiation. Online supplemental material is available at http://www.jcb.org/cgi/content/full/jcb.200503043/DC1.

We thank Yasuhisa Adachi, Thanos Halazonetis, Manuel Stucki, Stephen Jackson, and Yossi Shiloh for reagents and Manuel Stucki for fruitful discussions.

This work was supported by grants from the Danish Cancer Society (DP 03 035), Danish National Research Foundation, European Union (DNA Repair 512113), European Science Foundation (EuroDYNA 21-04-280), and John and Birthe Meyer Foundation.

Submitted: 8 March 2005
Accepted: 6 June 2005

References

Anderson, L., C. Henderson, and Y. Adachi. 2001. Phosphorylation and rapid relocalization of 53BP1 to nuclear foci upon DNA damage. *Mol. Cell. Biol.* 21:1719–1729.

Celeste, A., O. Fernandez-Capetillo, M.J. Kruhlak, D.R. Pilch, D.W. Staudt, A. Lee, R.F. Bonner, W.M. Bonner, and A. Nussenzweig. 2003. Histone H2AX phosphorylation is dispensable for the initial recognition of DNA breaks. *Nat. Cell Biol.* 5:675–679.

D'Amours, D., and S.P. Jackson. 2002. The Mre11 complex: at the crossroads of DNA repair and checkpoint signalling. *Nat. Rev. Mol. Cell Biol.* 3:317–327.

DiTullio, R.A., Jr., T.A. Mochan, M. Venere, J. Bartkova, M. Sehested, J. Bartek, and T.D. Halazonetis. 2002. 53BP1 functions in an ATM-dependent checkpoint pathway that is constitutively activated in human cancer. *Nat. Cell Biol.* 4:998–1002.

Downs, J.A., S. Allard, O. Jobin-Robitaille, A. Javaheri, A. Auger, N. Bouchard, S.J. Kron, S.P. Jackson, and J. Cote. 2004. Binding of chromatin-modifying activities to phosphorylated histone H2A at DNA damage sites. *Mol. Cell.* 16:979–990.

Durocher, D., S.J. Smerdon, M.B. Yaffe, and S.P. Jackson. 2000. The FHA domain in DNA repair and checkpoint signaling. *Cold Spring Harb. Symp. Quant. Biol.* 65:423–431.

Essers, J., A.B. Houtsmuller, L. van Veelen, C. Paulusma, A.L. Nigg, A. Pastink, W. Vermeulen, J.H. Hoeijmakers, and R. Kanaar. 2002. Nuclear dynamics of RAD52 group homologous recombination proteins in response to DNA damage. *EMBO J.* 21:2030–2037.

Falck, J., J.H. Petrini, B.R. Williams, J. Lukas, and J. Bartek. 2002. The DNA damage-dependent intra-S phase checkpoint is regulated by parallel pathways. *Nat. Genet.* 30:290–294.

Falck, J., J. Coates, and S.P. Jackson. 2005. Conserved modes of recruitment of ATM, ATR and DNA-PKcs to sites of DNA damage. *Nature.* 434:605–611.

Fernandez-Capetillo, O., H.T. Chen, A. Celeste, I. Ward, P.J. Romanienko, J.C. Morales, K. Naka, Z. Xia, R.D. Camerini-Otero, N. Motoyama, et al. 2002. DNA damage-induced G2-M checkpoint activation by histone H2AX and 53BP1. *Nat. Cell Biol.* 4:993–997.

Fernandez-Capetillo, O., C.D. Allis, and A. Nussenzweig. 2004. Phosphorylation of histone H2B at DNA double-strand breaks. *J. Exp. Med.* 199:1671–1677.

Goldberg, M., M. Stucki, J. Falck, D. D'Amours, D. Rahman, D. Pappin, J. Bartek, and S.P. Jackson. 2003. MDC1 is required for the intra-S-phase DNA damage checkpoint. *Nature.* 421:952–956.

Houtsmuller, A.B., S. Rademakers, A.L. Nigg, D. Hoogstraten, J.H. Hoeijmakers, and W. Vermeulen. 1999. Action of DNA repair endonuclease ERCC1/XPF in living cells. *Science.* 284:958–961.

Huyen, Y., O. Zgheib, R.A. Ditullio Jr., V.G. Gorgoulis, P. Zacharatos, T.J. Petty, E.A. Sheston, H.S. Mellert, E.S. Stavridi, and T.D. Halazonetis. 2004. Methylated lysine 79 of histone H3 targets 53BP1 to DNA double-strand breaks. *Nature.* 432:406–411.

Iwabuchi, K., P.L. Bartel, B. Li, R. Marraccino, and S. Fields. 1994. Two cellular proteins that bind to wild-type but not mutant p53. *Proc. Natl. Acad. Sci. USA.* 91:6098–6102.

Jullien, D., P. Vagnarelli, W.C. Earnshaw, and Y. Adachi. 2002. Kinetochore localisation of the DNA damage response component 53BP1 during mitosis. *J. Cell Sci.* 115:71–79.

Kastan, M.B., and J. Bartek. 2004. Cell-cycle checkpoints and cancer. *Nature.* 432:316–323.

Leung, T.K., M.Y. Rajendran, C. Monfries, C. Hall, and L. Lim. 1990. The human heat-shock protein family. Expression of a novel heat-inducible HSP70 (HSP70B') and isolation of its cDNA and genomic DNA. *Biochem. J.* 267:125–132.

Li, G., M. Levitus, C. Bustamante, and J. Widom. 2005. Rapid spontaneous accessibility of nucleosomal DNA. *Nat. Struct. Mol. Biol.* 12:46–53.

Lisby, M., J.H. Barlow, R.C. Burgess, and R. Rothstein. 2004. Choreography of the DNA damage response: spatiotemporal relationships among checkpoint and repair proteins. *Cell.* 118:699–713.

Lou, Z., C.C. Chini, K. Minter-Dykhouse, and J. Chen. 2003a. Mediator of DNA damage checkpoint protein 1 regulates BRCA1 localization and phosphorylation in DNA damage checkpoint control. *J. Biol. Chem.* 278:13599–13602.

Lou, Z., K. Minter-Dykhouse, X. Wu, and J. Chen. 2003b. MDC1 is coupled to activated CHK2 in mammalian DNA damage response pathways. *Nature.* 421:957–961.

Lukas, C., J. Falck, J. Bartkova, J. Bartek, and J. Lukas. 2003. Distinct spatiotemporal dynamics of mammalian checkpoint regulators induced by DNA damage. *Nat. Cell Biol.* 5:255–260.

Lukas, C., F. Melander, M. Stucki, J. Falck, S. Bekker-Jensen, M. Goldberg, Y. Lerenthal, S.P. Jackson, J. Bartek, and J. Lukas. 2004a. Mdc1 couples DNA double-strand break recognition by Nbs1 with its H2AX-dependent chromatin retention. *EMBO J.* 23:2674–2683.

Lukas, J., C. Lukas, and J. Bartek. 2004b. Mammalian cell cycle checkpoints: signalling pathways and their organization in space and time. *DNA Repair (Amst.).* 3:997–1007.

Manke, I.A., D.M. Lowery, A. Nguyen, and M.B. Yaffe. 2003. BRCT repeats as phosphopeptide-binding modules involved in protein targeting. *Science.* 302:636–639.

Mochan, T.A., M. Venere, R.A. DiTullio Jr., and T.D. Halazonetis. 2003.

53BP1 and NFBD1/MDC1-Nbs1 function in parallel interacting pathways activating ataxia-telangiectasia mutated (ATM) in response to DNA damage. *Cancer Res.* 63:8586–8591.

Mochan, T.A., M. Venere, R.A. DiTullio Jr., and T.D. Halazonetis. 2004. 53BP1, an activator of ATM in response to DNA damage. *DNA Repair (Amst.).* 3:945–952.

Morales, J.C., Z. Xia, T. Lu, M.B. Aldrich, B. Wang, C. Rosales, R.E. Kellems, W.N. Hittelman, S.J. Elledge, and P.B. Carpenter. 2003. Role for the BRCA1 C-terminal repeats (BRCT) protein 53BP1 in maintaining genomic stability. *J. Biol. Chem.* 278:14971–14977.

Morrison, A.J., J. Highland, N.J. Krogan, A. Arbel-Eden, J.F. Greenblatt, J.E. Haber, and X. Shen. 2004. INO80 and gamma-H2AX interaction links ATP-dependent chromatin remodeling to DNA damage repair. *Cell.* 119:767–775.

Nyberg, K.A., R.J. Michelson, C.W. Putnam, and T.A. Weinert. 2002. Toward maintaining the genome: DNA damage and replication checkpoints. *Annu. Rev. Genet.* 36:617–656.

Peng, A., and P.L. Chen. 2003. NFBD1, like 53BP1, is an early and redundant transducer mediating Chk2 phosphorylation in response to DNA damage. *J. Biol. Chem.* 278:8873–8876.

Phair, R.D., P. Scaffidi, C. Elbi, J. Vecerova, A. Dey, K. Ozato, D.T. Brown, G. Hager, M. Bustin, and T. Misteli. 2004. Global nature of dynamic protein-chromatin interactions in vivo: three-dimensional genome scanning and dynamic interaction networks of chromatin proteins. *Mol. Cell. Biol.* 24:6393–6402.

Rogakou, E.P., C. Boon, C. Redon, and W.M. Bonner. 1999. Megabase chromatin domains involved in DNA double-strand breaks in vivo. *J. Cell Biol.* 146:905–916.

Schmiedeberg, L., K. Weisshart, S. Diekmann, G. Meyer Zu Hoerste, and P. Hemmerich. 2004. High- and low-mobility populations of HP1 in heterochromatin of mammalian cells. *Mol. Biol. Cell.* 15:2819–2833.

Schultz, L.B., N.H. Chehab, A. Malikzay, and T.D. Halazonetis. 2000. p53 binding protein 1 (53BP1) is an early participant in the cellular response to DNA double-strand breaks. *J. Cell Biol.* 151:1381–1390.

Shiloh, Y. 2003. ATM and related protein kinases: safeguarding genome integrity. *Nat. Rev. Cancer.* 3:155–168.

Stewart, G.S., B. Wang, C.R. Bignell, A.M. Taylor, and S.J. Elledge. 2003. MDC1 is a mediator of the mammalian DNA damage checkpoint. *Nature.* 421:961–966.

Stucki, M., and S.P. Jackson. 2004. MDC1/NFBD1: a key regulator of the DNA damage response in higher eukaryotes. *DNA Repair (Amst.).* 3:953–957.

Syljuasen, R.G., C.S. Sorensen, J. Nylandsted, C. Lukas, J. Lukas, and J. Bartek. 2004. Inhibition of Chk1 by CEP-3891 accelerates mitotic nuclear fragmentation in response to ionizing radiation. *Cancer Res.* 64:9035–9040.

Tashiro, S., J. Walter, A. Shinohara, N. Kamada, and T. Cremer. 2000. Rad51 accumulation at sites of DNA damage and in postreplicative chromatin. *J. Cell Biol.* 150:283–291.

van Attikum, H., O. Fritsch, B. Hohn, and S.M. Gasser. 2004. Recruitment of the INO80 complex by H2A phosphorylation links ATP-dependent chromatin remodeling with DNA double-strand break repair. *Cell.* 119:777–788.

Wang, B., S. Matsuoka, P.B. Carpenter, and S.J. Elledge. 2002. 53BP1, a mediator of the DNA damage checkpoint. *Science.* 298:1435–1438.

Ward, I.M., K. Minn, K.G. Jorda, and J. Chen. 2003a. Accumulation of checkpoint protein 53BP1 at DNA breaks involves its binding to phosphorylated histone H2AX. *J. Biol. Chem.* 278:19579–19582.

Ward, I.M., K. Minn, J. van Deursen, and J. Chen. 2003b. p53 binding protein 53BP1 is required for DNA damage responses and tumor suppression in mice. *Mol. Cell. Biol.* 23:2556–2563.

Xu, X., and D.F. Stern. 2003. NFBD1/MDC1 regulates ionizing radiation-induced focus formation by DNA checkpoint signaling and repair factors. *FASEB J.* 17:1842–1848.

Yu, X., C.C. Chini, M. He, G. Mer, and J. Chen. 2003. The BRCT domain is a phospho-protein binding domain. *Science.* 302:639–642.

Zhou, B.B., and S.J. Elledge. 2000. The DNA damage response: putting checkpoints in perspective. *Nature.* 408:433–439.